Influence of glycoprotein MUC1 on trafficking of the Ca²⁺-selective ion channels, TRPV5 and TRPV6, and on *in vivo* calcium homeostasis

Mohammad M. Al-bataineh[1], Carol L. Kinlough[1], Allison Marciszyn[1], Tracey Lam[1], Lorena Ye[1], Kendrah Kidd[2,3], Joseph C. Maggiore[4], Paul A. Poland[1], Stanislav Kmoch[2,3], Anthony Bleyer[2,3], Daniel J. Bain[5], Nicolas Montalbetti[1], Thomas R. Kleyman[1,6,7], Rebecca P. Hughey[1,6,*], and Evan C. Ray[1]

From the [1]Renal-Electrolyte Division, Department of Medicine, University of Pittsburgh, Pittsburgh, Pennsylvania, USA; [2]Section on Nephrology, Department of Medicine, Wake Forest University, Winston-Salem, North Carolina, USA; [3]Department of Paediatrics and Inherited Metabolic Disorders, First Faculty of Medicine, Charles University, Prague, Czech Republic; [4]Department of Developmental Biology, [5]Department of Geology and Environmental Science, [6]Department of Cell Biology, and [7]Department of Pharmacology and Chemical Biology, University of Pittsburgh, Pittsburgh, Pennsylvania, USA

Polymorphism of the gene encoding mucin 1 (*MUC1*) is associated with skeletal and dental phenotypes in human genomic studies. Animals lacking MUC1 exhibit mild reduction in bone density. These phenotypes could be a consequence of modulation of bodily Ca homeostasis by MUC1, as suggested by the previous observation that MUC1 enhances cell surface expression of the Ca²⁺-selective channel, TRPV5, in cultured unpolarized cells. Using biotinylation of cell surface proteins, we asked whether MUC1 influences endocytosis of TRPV5 and another Ca²⁺-selective TRP channel, TRPV6, in cultured polarized epithelial cells. Our results indicate that MUC1 reduces endocytosis of both channels, enhancing cell surface expression. Further, we found that mice lacking MUC1 lose apical localization of TRPV5 and TRPV6 in the renal tubular and duodenal epithelium. Females, but not males, lacking MUC1 exhibit reduced blood Ca²⁺. However, mice lacking MUC1 exhibited no differences in basal urinary Ca excretion or Ca retention in response to PTH receptor signaling, suggesting compensation by transport mechanisms independent of TRPV5 and TRPV6. Finally, humans with autosomal dominant tubulointerstitial kidney disease due to frame-shift mutation of *MUC1* (ADTKD-MUC1) exhibit reduced plasma Ca concentrations compared to control individuals with mutations in the gene encoding uromodulin (ADTKD-UMOD), consistent with MUC1 haploinsufficiency causing reduced bodily Ca²⁺. In summary, our results provide further insight into the role of MUC1 in Ca²⁺-selective TRP channel endocytosis and the overall effects on Ca concentrations.

Mucin 1 (MUC1) is a heavily glycosylated, single transmembrane protein, expressed at the apical surface of many epithelial cells. Previous studies have demonstrated that MUC1 enhances cell surface expression and electrical activity of the Ca²⁺-selective channel, TRPV5, *in vitro* (1). In this

article, we ask whether MUC1 influences subcellular localization of TRPV5 *in vivo*, whether MUC1 influences activity of other Ca²⁺-selective ion channels (TRPV6), *how* MUC1 influences cellular trafficking of TRP channels, and whether MUC1 deficiency exerts an *in vivo* influence on Ca²⁺ homeostasis.

Human observational studies suggest MUC1 could participate in Ca²⁺ homeostasis. Genetic analyses find an association between *MUC1* and numerous skeletal phenotypes including heel bone mineral density ($p = 1.4 \times 10^{-13}$) (2), estimated bone density from heel ultrasound ($p = 1 \times 3.9 \times 10^{-11}$) (3), estimated bone mineral density (2.1×10^{-6}) (4), femoral neck bone mineral density (1.5×10^{-4}) (5), bone mineral density in older people (4.8×10^{-4}) (6), standing height ($p = 1.5 \times 10^{-7}$) (7), childhood height ($p = 1.6 \times 10^{-4}$) (7), and need for dentures ($p = 4.2 \times 10^{-10}$) (7). Urinary MUC1 excretion is associated with the presence of hypercalciuria and calcium nephrolithiasis (1). Though these studies demonstrate an association between *MUC1* and traits that are influenced by Ca²⁺ homeostasis, this association does not explain how MUC1 could influence Ca²⁺ homeostasis.

One clue comes from the observation that MUC1 is expressed in several epithelia that are specialized for transcellular Ca²⁺ transport (8, 9). In the kidney, MUC1 is expressed in the thick ascending limb, distal convoluted tubule, connecting tubule, and collecting duct (10). The distal convoluted tubule and connecting tubule participate in transcellular Ca²⁺ absorption through the activity of transient receptor potential cation channel subfamily V members 5 and 6 (TRPV5 and TRPV6, previously referred to as ECaC1 and ECaC2, respectively). In the GI tract, TRPV6 and MUC1 are coexpressed in duodenum, ileum, and colon, where transcellular Ca²⁺ uptake also occurs (11, 12).

MUC1 physically interacts with TRPV5, as demonstrated by the ability of these proteins to coimmunoprecipitate (1). Furthermore, MUC1 enhances cell surface expression and activity of TRPV5 in cultured fibroblasts. The ability of MUC1

to increase cell surface expression of TRPV5 is dependent upon a single N-glycan in TRPV5 (N358 in the human ortholog) and upon expression of galectin-3, which is suggested to physically mediate the interaction between MUC1 and TRPV5. The ability of MUC1 to enhance activity of TRPV5 depends upon both dynamin and caveolin, suggesting that MUC1 enhances cell surface expression of TRPV5 by impairing endocytosis, at least in fibroblasts.

As the Asn residue in TRPV5 that is required for MUC1-dependent upregulation of channel activity is conserved in TRPV6, we also ask whether MUC1 influences subcellular localization of TRPV6 *in vivo*. Further, does MUC1 influence the rate of TRPV6 endocytosis in polarized epithelial cells (Madin-Darby canine kidney cells, MDCK)?

We examine MUC1-deficient animals to determine whether they exhibit altered Ca homeostasis. Finally, we evaluate Ca^{2+} levels in patients with *MUC1* mutation causing autosomal dominant, tubulointerstitial kidney disease (ADTKD-MUC1) to determine whether *MUC1* mutation results in haploinsufficiency, causing reduced blood Ca^{2+} levels as compared to control patients with autosomal dominant, tubulointerstitial kidney disease due to mutation in *UMOD*, encoding uromodulin (ADTKD-UMOD).

Results

MUC1 was previously shown to enhance cell surface expression of TRPV5 in a dynamin and caveolin-1–dependent fashion in fibroblasts, consistent with an influence on channel endocytosis. We asked whether MUC1 enhances cell surface expression of channels in polarized epithelial cells, using cell surface biotinylation of proteins in MDCK cells with, and without, stable overexpression of MUC1. We confirmed that MUC1 enhances cell surface expression of TRPV5 in polarized epithelial cells in culture (Fig. 1A). Stable expression of MUC1 in MDCK cells increased TRPV5 cell surface expression (5.29 ± 0.71% with MUC1 *versus* 4.22 ± 0.45% without MUC1, N = 4 for each, $p < 0.05$ by Student's t test). The increase in cell surface expression was associated with significantly decreased rates of TRPV5 endocytosis in cells with MUC1 ($p < 0.01$ by two-way ANOVA).

The percentage of TRPV6 at the cell surface in the presence of MUC1 (7.08 ± 2.89%, N = 10) was also significantly different than in the absence of MUC1 (4.34 ± 2.18%, N = 8, $p < 0.05$ by Student's t test) (Fig. 1B). As with TRPV5, MUC1 significantly retarded endocytosis of TRPV6 ($p < 0.001$ by two-way ANOVA). In the presence of MUC1, endocytosis of these channels resembles that of MUC1 itself. In contrast, MUC1 coexpression does not alter endocytosis rate of the endogenous cell surface protein podocalyxin (Fig. 1C).

We used the patch-clamp technique in whole cell configuration to evaluate the effect of MUC1 on TRPV6-mediated currents. Calcium influx was detected by monitoring inward currents at −80 mV during voltage ramps. Inwardly rectifying currents were observed in TRPV6-expressing HEK293 cells in the presence of 2 mM Ca^{2+} (Fig. 2), while no such currents were detected in the absence of Ca^{2+} or in WT HEK293 cells

(not shown). Consistent with the observed effect of MUC1 on TRPV6 plasma membrane abundance, HEK293 cells coexpressing TRPV6 with MUC1 exhibited a 2.6-fold increase in current density when compared with controls expressing TRPV6 alone ($p < 0.05$ by Student's t test).

Having confirmed that MUC1 slows endocytosis and enhances cell surface expression of both TRPV5 and TRPV6 in polarized cells in culture, we then asked whether MUC1 influences subcellular localization of these channels *in vivo*. Kidney and duodenum sections from $Muc1^{-/-}$ or from $Muc1^{+/+}$ littermate control mice were immunostained for TRPV5 and TRPV6 (Fig. 3). In kidney, both TRPV5 and TRPV6 are redistributed from the cell apex toward the cytoplasm in $Muc1^{-/-}$ mice ($p < 0.0001$ by Student's t test for cytoplasm/apical staining for both TRPV5 and TRPV6 in kidney). Similarly, in duodenum, apical localization of TRPV6 is lost in $Muc1^{-/-}$ animals ($p < 0.0001$ by Student's t test for cytoplasm/apical staining).

TRPV5 and TRPV6 KO animals exhibit systemic Ca^{2+} depletion as a consequence of impaired transcellular Ca^{2+} transport in the intestine and kidney tubule (13, 14). We asked whether $Muc1^{-/-}$ mice exhibit reduced whole blood concentrations of Ca^{2+} and other electrolytes (Fig. 4 and Table 1). Blood Ca^{2+} levels were significantly lower in female $Muc1^{-/-}$ mice (1.17 ± 0.06, N = 6) than in $Muc1^{+/+}$ females (1.23 ± 0.03, N = 10; $p < 0.05$). Male mice had similar blood Ca^{2+} in $Muc1^{+/+}$ (1.20 ± 0.03, N = 13) *versus* Muc1$^{-/-}$ animals (1.20 ± 0.06, N = 12; p = NS).

To examine whether MUC1 deficiency causes urinary wasting of Ca, we measured urinary Ca excretion ($U_{Ca}\dot{V}$) of mice in metabolic cages (Fig. 4). Over 3.5 h, Muc1$^{+/+}$ mice excreted 0.87 ± 0.35 μg/h/g body weight (N = 31) compared to 0.71 ± 0.27 (N = 27) in $Muc1^{-/-}$ mice (p = NS). No differences were observed when mice were stratified on the basis of sex: male WT littermates excreted 0.77 ± 0.27 (N = 18) and $Muc1^{-/-}$ males excreted 0.73 ± 0.32 (N = 16, p = NS); female WT littermates excreted 1.0 ± 0.41 (N = 13) and female $Muc1^{-/-}$ mice excreted 0.67 ± 0.18 (N = 11, p = NS) μg/h/g body weight. There were also no differences in urinary Na or K excretion (not shown).

To examine whether $Muc1^{-/-}$ mice compensated for reduced transcellular transport by upregulating active vitamin D or parathyroid hormone (PTH) production, plasma 1,25(OH)$_2$ vitamin D and PTH were measured in $Muc1^{-/-}$ mice and in $Muc1^{+/+}$ littermates. Plasma levels of 1,25(OH)$_2$ Vitamin D did not differ in $Muc1^{+/+}$ (103 ± 13 pg/ml, N = 16) *versus* $Muc1^{-/-}$ mice (105 ± 17, N = 20; p = NS). No differences were observed after stratification of mice by sex. In males, WT littermates exhibited plasma 1,25(OH)$_2$ Vitamin D of 108 ± 14 pg/ml (N = 8) compared to 114 ± 17 (N = 11; p = NS). In females, levels in WT littermates were 98 ± 11 (N = 8) compared to 95 ± 10 pg/ml (N = 9; p = NS). PTH levels were not different in $Muc1^{-/-}$ *versus* littermate control mice. Overall, PTH levels were 228 ± 86 pg/ml in littermate control animals (N = 30) and 193 ± 33 in Muc1$^{-/-}$ animals (N = 24, p = NS). In males, these were 250 ± 108 (N = 16) in littermates and 193 ± 33 (N = 15, p = NS) in Muc1$^{-/-}$ mice. In females, these were 202 ± 41 (N = 14) and 193 ± 34 (N = 9, p = NS) in littermates and Muc1$^{-/-}$ mice, respectively.
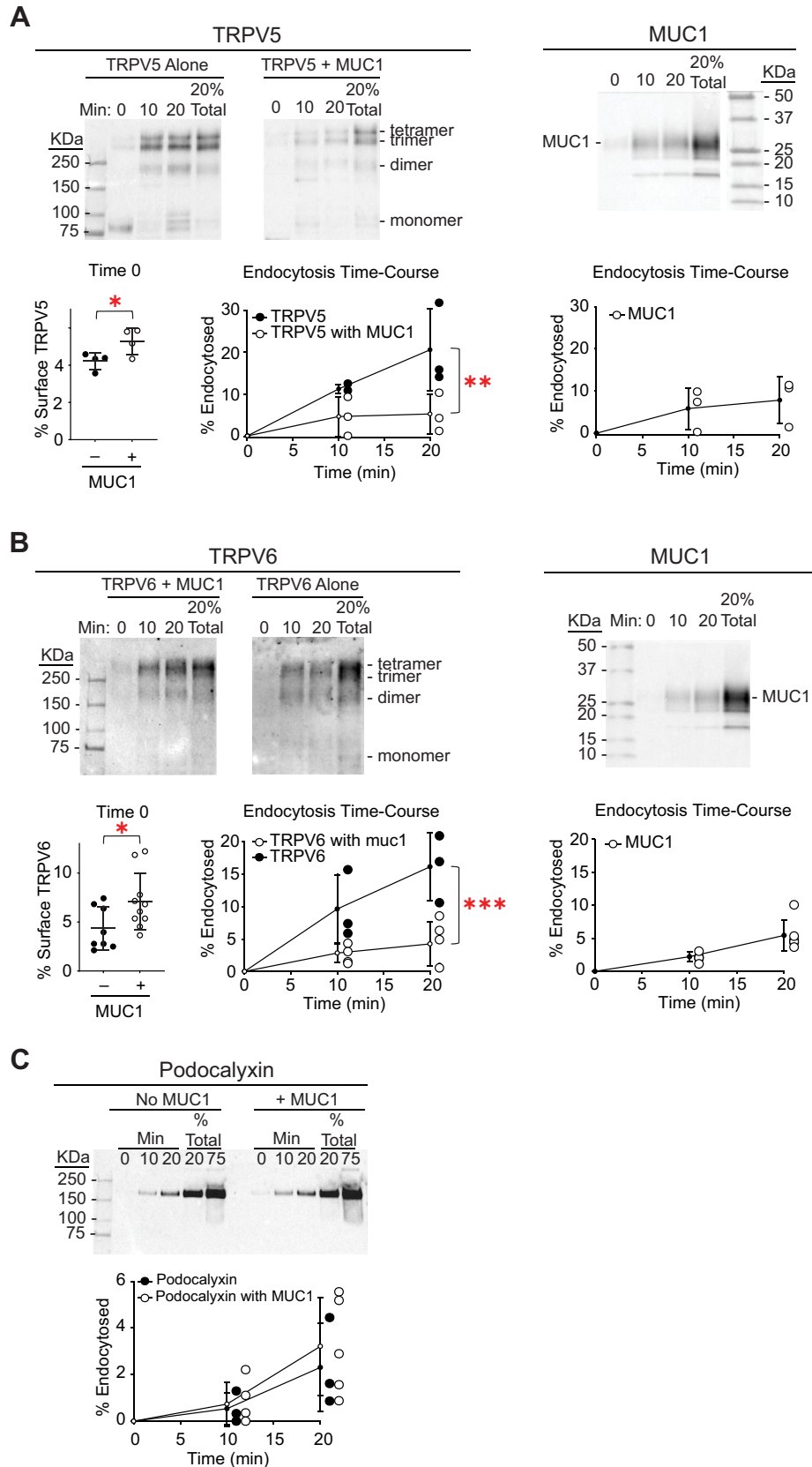
A

B

C

Figure 1. MUC1 increases cell surface expression and decreases rates of endocytosis selectively for TRPV5 and TRPV6 in polarized epithelial cells.
A, cell surface expression and endocytosis of TRPV5 were examined. MDCK cells with, or without, stable expression of MUC1 were transiently transfected with TRPV5-GFP. Cell surface proteins were labeled with membrane-impermeant sulfo-NHS-SS-biotin on ice and moved to a circulating water bath at 37 °C for 0, 10, or 20 min. Cells were returned to ice, and surface biotin was stripped with MESNA. Cell lysates were incubated overnight at 4 °C with neutravidin-conjugated beads. Beads were washed and proteins eluted in sample buffer with β-mercaptoethanol at 60 °C for 5 min before SDS-PAGE and

A Patch-clamp voltage protocol
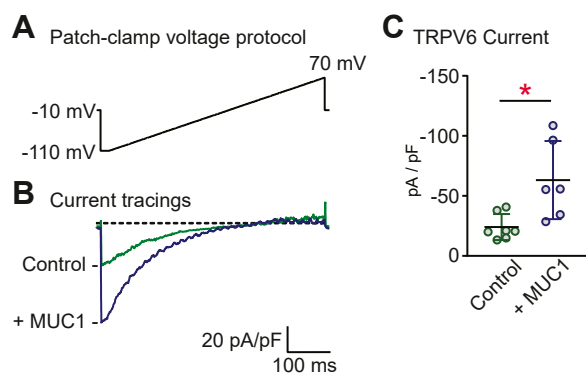
B Current tracings

C TRPV6 Current

Figure 2. MUC1 increases TRPV6 whole cell current density. *A*, whole cell currents were evoked by linear ramps from −100 to 70 mV from a holding potential of −10 mV as described in Experimental procedures. *B*, typical current traces are shown after maximal activation for HEK293 cells transfected with TRPV6 or cells cotransfected with TRPV6 and MUC1. The *dashed line* represents zero current. *C*, summary of the effect of MUC1 on TRPV6-mediated whole cell currents measured at −80 mV. Cotransfection of MUC1 resulted in increased TRPV6 current density (−63 ± 13 pA/pF, n = 6, compared with controls expressing TRPV6 alone (−24 ± 4 pA/pF, n = 7)). Data are presented as means ± SEM (*$p < 0.05$ by Student's *t* test).

PTH upregulates TRPV5 cell surface expression by reducing caveolin-1–mediated endocytosis of the channel [15]. Because MUC1 modulates endocytosis of TRPV5 and TRPV6 in cultured cells, responsiveness of $Muc1^{-/-}$ mice to a stable PTH analog (teriparatide, TPT) as compared to vehicle (normal saline solution, NSS) was examined (Fig. 5.) In both genotypes, TPT accelerated urinary phosphorus excretion ($U_{Phos}\dot{V}$, $p < 0.0001$) while delaying urinary Ca excretion ($U_{Ca}\dot{V}$, $p < 0.0001$) compared to excretion rates following NSS alone. The genotype-treatment interaction term was not significant by mixed effects modeling (p = NS). TPT acutely increases blood Ca^{2+}, predominantly by increasing bone turn-over [16]. Differences in blood Ca^{2+} could influence Ca^{2+} filtration and $U_{Ca}\dot{V}$. Additional mice were treated with TPT and sacrificed to confirm that TPT had similar effects on blood Ca^{2+} in $Muc1^{+/+}$ and $Muc1^{-/-}$ mice. Blood Ca^{2+} was similar in TPT-treated $Muc1^{+/+}$ (1.35 ± 0.05 mmol/l; N = 19) and $Muc1^{-/-}$ (1.38 ± 0.06 mmol/l; N = 12; p = NS) mice.

To examine whether MUC1 influences Ca homeostasis in humans, plasma Ca was assessed in individuals with one working copy of *MUC1*. Autosomal dominant tubulointerstitial kidney disease can occur as a consequence of a frameshift mutation in *MUC1* (ADTKD-MUC1) or mutation in the gene encoding uromodulin (*UMOD*, ADTKD-UMOD) [17]. Both result in the slow progression of interstitial fibrosis, with indolent loss of glomerular filtration with mean age of end stage kidney disease in the fifth decade of life.

Plasma total Ca levels (ionized Ca^{2+} plus nonionized, as is commonly measured in clinical laboratories) were compared from individuals genetically determined to have either ADTKD-MUC1 or ADTKD-UMOD. Only individuals with a glomerular filtration rate of at least 60 ml/min were examined. Overall, plasma Ca was lower in individuals with ADTKD-MUC1 than with ADTKD-UMOD (Fig. 6). ADTKD-UMOD patients exhibited Ca of 9.58 ± 0.38 mg/dl (N = 72), compared to 9.41 ± 0.40 in ADTKD-MUC1 patients (N = 73; $p < 0.01$ by Student's *t* test). After stratification on the basis of sex, lower serum Ca concentrations remained significant in women but not men. Men with ADTKD-UMOD exhibited Ca of 9.70 ± 0.43 (N = 27), compared to men with ADTKD-MUC1, who had Ca of 9.50 ± 0.40 (N = 33; p = NS). In women, those with ADTKD-UMOD had Ca of 9.51 ± 0.32 (N = 45) as compared to 9.34 ± 0.40 in those with ADTKD-MUC1 (N = 40; $p < 0.05$).

Discussion

Findings presented above add to evidence demonstrating a role for MUC1 in Ca^{2+} homeostasis. (i) $Muc1^{-/-}$ mice exhibit reduced apical localization of both TRPV5 and TRPV6, which are critical for transcellular Ca^{2+} absorption in renal tubules and intestines. (ii) $Muc1^{-/-}$ mice exhibit lower blood Ca^{2+}. Interestingly, $Muc1^{-/-}$ mice exhibited no difference in urinary Ca^{2+} excretion. This could reflect a state of Ca homeostasis, albeit with lower systemic Ca stores. (iii) A previous study found mild reduction in bone density in $Muc1^{-/-}$ mice [18]. Osteoblast and osteoclast function appeared normal in $Muc1^{-/-}$ mice, and no compelling mechanism for the bone phenotype was described. Altered Ca^{2+} handling was not examined but provides a good explanation for the observed bone phenotype. (iv) A common *MUC1* polymorphism (rs4072037) is associated with altered bone density in humans [19, 20]. (v) Patients with ADTKD-MUC1, who have a frameshift–inducing mutation in *MUC1*, exhibit lower levels of circulating Ca^{2+} than individuals with ADTKD-UMOD. This is somewhat surprising, given that UMOD contributes to mineral transport in the thick ascending limb, including through support of NKCC2 activity [21]. Because pharmacologic impairment of NKCC2 activity induces urinary Ca^{2+} wasting [22, 23], reduced NKCC2 activity in ADTKD-UMOD might be expected to reduce blood Ca^{2+}. The observation that blood Ca^{2+} levels in ADTKD-MUC1 are lower is consistent with Ca^{2+} depletion through reduced cell surface localization of Ca^{2+}-selective channels, though other mechanisms could contribute. The difference in blood Ca^{2+} observed in these

immunoblotting for either TRPV5 with anti-GFP antibodies or for MUC1 with anti-cytoplasmic tail (CT2) antibodies. Differences in the oligomerization state of TRPV5-GFP were the result of the overnight incubation at 4 °C and not indicative of changes *in situ* (see Fig. S1). Therefore, all oligomerization states were included for the quantification of TRPV5-GFP. Time 0 represents basal cell surface expression of TRPV5. MUC1 increased TRPV5 cell surface expression (28%, *$p < 0.05$ by Student's *t* test). Endocytosis time-courses (N = 3) show that MUC1 reduces TRPV5 endocytosis (**$p < 0.01$ by two-way ANOVA). Endocytosis of TRPV5 in the presence of MUC1 did not differ significantly from that of MUC1 itself. Representative blots are shown for each analysis. *B*, cell surface expression and endocytosis time-course of TRPV6 with, and without, coexpression with MUC1 were examined as in (*A*). Blots were developed with rabbit anti-TRPV6 or anti-MUC1 cytoplasmic tail antibodies. Time 0–biotinylated TRPV6 demonstrated increased basal cell surface TRPV6 in the presence of MUC1 (63%, *$p < 0.05$ by Student's *t* test). MUC1 coexpression significantly reduced TRPV6 endocytosis (***$p = 0.001$ by two-way ANOVA). Endocytosis of TRPV6 in the presence of MUC1 did not differ significantly from that of MUC1 itself. Representative blots are shown for each analysis. *C*, endocytosis of an endogenous protein, podocalyxin, in MDCK cells is no different in the presence or absence of MUC1 expression (p = NS by two-way ANOVA). Representative blots are shown for each analysis. Error bars represent SD of the mean. MDCK, Madin-Darby canine kidney.
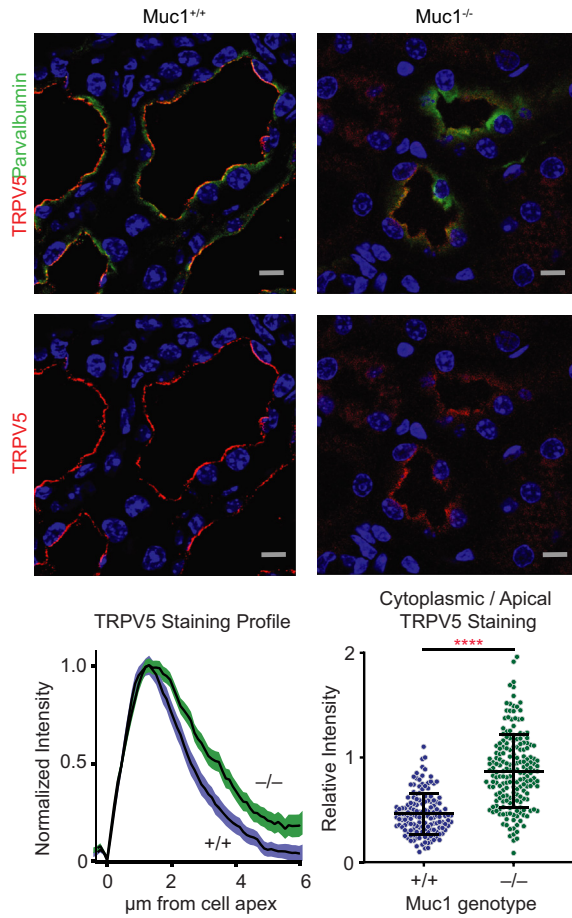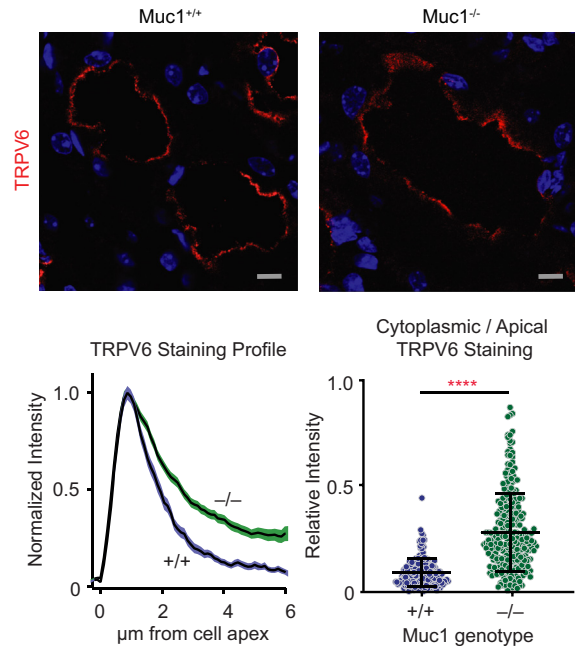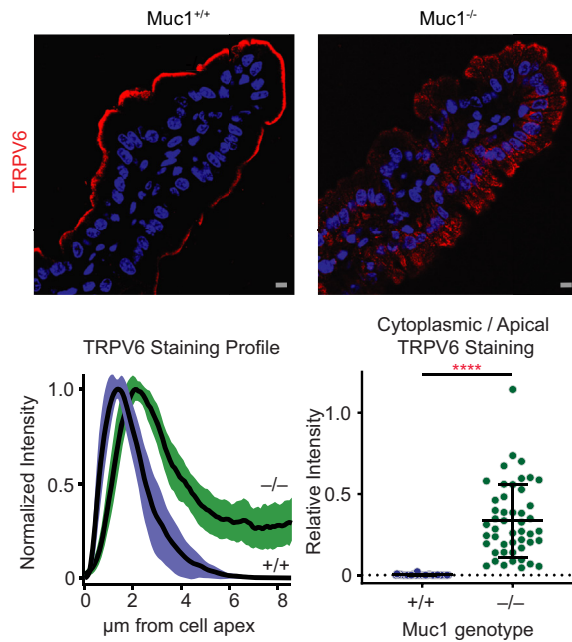
Figure 3. Absence of MUC1 *in vivo* shifts localization of TRPV5 and TRPV6 away from the cell apex. *A*, representative immunofluorescence images show redistribution of TRPV5 from the renal tubule cell apex toward cytoplasm in kidneys from *Muc1*^{−/−} mice. *Red* represents TRPV5 staining. *Green* represents parvalbumin staining, indicating early distal convoluted tubule. *Blue* represents TO-PRO-3 staining. Panel below shows the mean of line scans of TRPV5 staining intensity from the cell surface, extending into the cytosol from *Muc1*^{−/−} mice and from *Muc1*^{+/+} controls (one line scan per TRPV5-expressing cell). Y-axis represents mean normalized intensity in early DCT epithelial cells. X-axis indicates distance from apparent cell surface. Shading behind *black line*
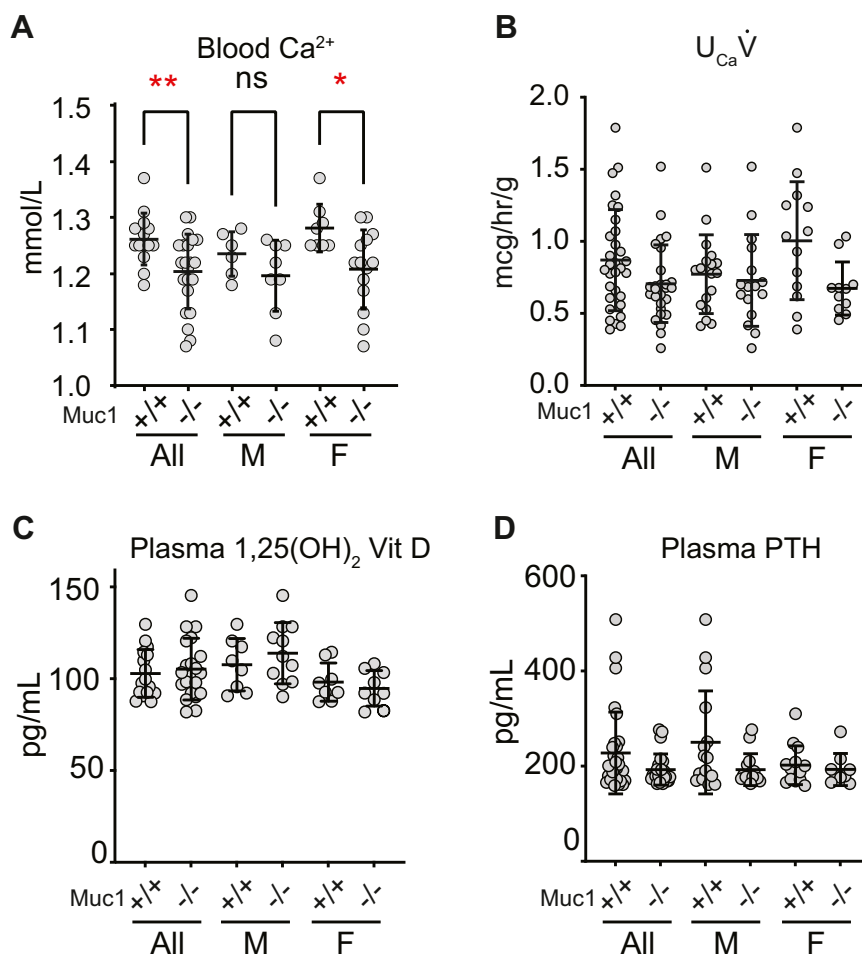
Figure 4. *Muc1*⁻/⁻ mice exhibit lower blood Ca²⁺, but no differences in Ca excretion. *A*, blood Ca²⁺ levels are lower in female but not male *Muc1*⁻/⁻ mice. Female *Muc1*⁻/⁻ mice exhibited lower blood Ca²⁺ than Muc1⁺/⁺ controls (*$p < 0.05$ and **$p < 0.01$ by Student's *t* test). Male mice had similar blood Ca²⁺ in Muc1⁺/⁺ controls compared to Muc1⁻/⁻ animals (p = NS). There was no genotype-specific difference when male and female mice were pooled (p = NS). *B*, urine Ca excretion rate (U_Ca V̇) was not different in *Muc1*⁻/⁻ mice compared to littermate controls. Urine was collected over 3.5 h in metabolic cages, and urinary Ca excretion (U_Ca V̇) was measured. No difference in U_Ca V̇ was observed overall (p = NS by Student's *t* test) or when mice were stratified on the basis of sex (p = NS in pairwise comparison by Student's *t* test). *C*, plasma levels of 1,25(OH)₂ Vitamin D did not differ in *Muc1*⁺/⁺ versus *Muc1*⁻/⁻ mice, either overall or after stratification by sex (p = NS in pairwise comparison by Student's *t* test). *D*, PTH levels were not different in *Muc1*⁺/⁺ versus *Muc1*⁻/⁻ mice either overall or after stratification by sex (p = NS in pairwise comparison by Student's *t* test). Error bars represent SD of the mean.

patients is mild, and hypocalcemia is not a recognized feature of ADTKD-MUC1. No published data address whether patients with ADTKD-MUC1 are at increased risk of bone disease associated with their chronic kidney disease.

Given the robust difference in TRP channel localization observed *in vivo* in kidney and duodenum, it is surprising that the measured parameters of Ca homeostasis—blood Ca²⁺, urine Ca excretion, PTH, and 1,25 (OH)2 vitamin D—are not more dramatically altered. Even the decrement in bone

mineralization previously observed in *Muc1*⁻/⁻ mice is relatively minor compared to the decrease in bone density that is observed in TRPV5⁻/⁻ or TRPV6⁻/⁻ mice as a consequence of systemic Ca depletion ([13], [14], [18]). There is also no evident divergence in bone density in *Muc1*⁻/⁻ mice compared with controls, as a function of age ([18]). All this suggests compensatory measures independent of these Ca²⁺-selective channels. It is possible that dietary stressors, such as prolonged Ca depletion, could reveal a more significant phenotype.

represents 95% confidence interval of line scans (N = 3 animals per genotype; n = 251 cells for *Muc1*⁺/⁺ mice; n = 332 cells for *Muc1*⁻/⁻ mice). Note, divergence of line scans within the cytoplasmic region, indicating more TRPV5 staining in the cytosol in *Muc1*⁻/⁻ mice. Second panel represents mean cytoplasm/apical staining intensity, as calculated from arbitrarily chosen cytosolic and apical cell regions. Cytoplasm/cell apex staining of TRPV5 is greater in *Muc1*⁻/⁻ mice (N = 3 animals per genotype, n = 147 cells for *Muc1*⁺/⁺ mice; n = 192 cells for *Muc1*⁻/⁻ mice; ****$p < 0.0001$ by Student's *t* test). *B*, TRPV6 subcellular localization in mouse kidney. *Red* represents TRPV6 staining. Panel below shows the mean of line scans of TRPV6 staining intensity. TRPV6 staining intensity is shifted away from the cell apex, toward cytoplasm (N = 3 animals per genotype, n = 180 cells for *Muc1*⁺/⁺ mice; n = 380 cells for *Muc1*⁻/⁻ mice). Adjacent panel shows cytoplasm/apical TRPV6 staining in tubular epithelial cells. Cytoplasm/apical TRPV6 staining is greater in *Muc1*⁻/⁻ mice (N = 3 animals per genotype; n = 184 cells for *Muc1*⁺/⁺ mice; n = 270 cells for *Muc1*⁻/⁻ mice; ****$p < 0.0001$ by Student's *t* test). *C*, duodenal epithelium TRPV6 staining is also shifted toward cytoplasm in *Muc1*⁻/⁻ mice. Line scans and cytoplasm/apical staining were examined from 5 to 10 cells per villus in 9 to 10 individual villi per duodenum from a total of three mice from each genotype (n = 45 cells for *Muc1*⁺/⁺ mice; n = 48 for *Muc1*⁻/⁻ mice). Line scans and cytoplasm/apical staining both show a shift of TRPV6 staining away from cell apex, toward the cytoplasm in *Muc1*⁻/⁻ mice (****$p < 0.0001$ by Student's *t* test). In all images, *gray* scale bars represent 10 μm. Error bars represent SD of the mean. DCT, distal convoluted tubule.

Table 1
Blood electrolytes

Sex	All		Male		Female	
Genotype	+/+	−/−	+/+	−/−	+/+	−/−
Na⁺	145 ± 1 (23)	145 ± 2 (17)	146 ± 1 (14)	145 ± 2 (11)	145 ± 2 (9)	145 ± 2 (6)
K⁺	4.6 ± 0.6 (23)	4.6 ± 0.2 (17)	4.7 ± 0.5 (14)	4.7 ± 0.2 (11)	4.5 ± 0.6 (9)	4.6 ± 0.3 (6)
Cl⁻	112 ± 2 (17)	112 ± 2 (17)	112 ± 3 (8)	111 ± 2 (11)	113 ± 2 (9)	113 ± 2 (6)
BUN	28 ± 4 (17)	27 ± 5 (17)	28 ± 3 (8)	27 ± 6 (11)	29 ± 4 (9)	26 ± 5 (6)

Cells show mean values (N). Na, K, and Cl units are in mmol/l. BUN: blood urea nitrogen, in mg/dl. No pairwise $Muc1^{+/+}$ *versus* $Muc1^{-/-}$ comparisons were statistically significant by Student's t test.

These data support a model in which transcellular Ca^{2+} transport is modulated by an extracellular protein lattice including MUC1, galectins, and ion channels that promotes cell surface expression of ion channels by opposing endocytosis. MUC1 enhances cell surface expression of TRPV5 in polarized epithelial cells in culture and increases apical expression of TRPV5 *in vivo*, consistent with previous findings that MUC1 promotes cell surface expression of the channel in fibroblasts (1). TRPV5 and its more broadly expressed homolog, TRPV6, share a conserved extracellular Asn residue (N438 in human TRPV5) that is N-glycosylated and is necessary for binding to galectin-3. TRPV5 exhibits galectin-binding selectivity, interacting with galectin-3, but not galectin-1. TRPV6 also depends upon MUC1 *in vivo* for apical expression. Galectin-3, through its pentameric C-terminal carbohydrate recognition domains, binds to extracellular glycans on numerous extracellular proteins (24). Among these are MUC1 and MUC2 (25). For its part, MUC1 function is also selective. It binds preferentially with galectin-3 and galectin-9 but less to galectin-1, -4, -7, or -8 (26). This specificity is underscored by the finding that MUC1 selectively reduces endocytosis of TRPV5 and TRPV6, while exerting no influence on podocalyxin. Podocalyxin (gp135) is a cell surface protein that interacts with galectin 8, but not galectin-1, -3, or -9 (27). Like MUC1, uromodulin promotes cell surface expression of TRPV5 by opposing channel endocytosis, through mechanisms that may resemble those seen for MUC1 and TRPV5 (28). All of these observations suggest that an extracellular lattice including MUC1, galectin-3, and TRPV5 and TRPV6 contributes to transcellular calcium transport.

The importance of this network in mammalian physiology is suggested by the observation that multiple genetic components originated in concert as mammals diverged from their ancestors. Mucins originated in early metazoans (29), but MUC1 arose in the earliest mammals from a precursor similar to MUC5 (30). TRPV5 and V6 arose when a common ancestral gene underwent duplication, also with the earliest mammals (31). Thus, it appears that these proteins play an important role in mammalian Ca physiology.

In what ways this extracellular glycoprotein network may be regulated to maintain Ca^{2+} balance remains a significant question. PTH enhances cell surface expression of TRPV5 by inhibiting its caveolin-1–mediated endocytosis (15). Because MUC1 also influences endocytosis of the channel, we predicted that $Muc1^{-/-}$ mice would exhibit diminished Ca^{2+} retention in response to PTH receptor activation. However, this was not observed, perhaps because other Ca^{2+} handling effects, such as paracellular Ca^{2+} reabsorption, predominated over the short course of this experiment.

In summary, the mucin MUC1 reduces endocytosis of the Ca-selective TRP channels TRPV5 and TRPV6 and promotes cell surface localization of these channels *in vivo*, contributing positively to Ca^{2+} homeostasis.

Experimental procedures

Endocytosis assays

MDCK (MDCK 2001) cells were obtained from Kai Simons in the European Molecular Biology Laboratory in Heidelberg. Cells were grown in Dulbecco's modified Eagle's medium-
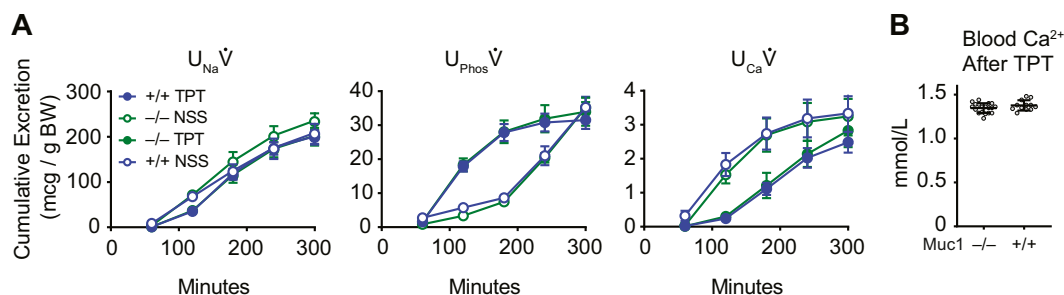

Figure 5. Urinary electrolyte excretion in response to the stable PTH analog, teriparatide, did not differ between $Muc1^{+/+}$ **and** $Muc1^{-/-}$ **mice.** *A*, urine Na excretion ($U_{Na}\dot{V}$), phosphorus excretion ($U_{Phos}\dot{V}$), and Ca excretion ($U_{Ca}\dot{V}$) were compared following injection of 5% volume/body weight of NSS. Two days later, the same animals received 5% volume/body weight of NSS with 150 µg/kg TPT. N = 8 $Muc1^{-/-}$ mice and 10 $Muc1^{+/+}$ mice. Open or closed symbols represent excretion following injection with NSS or TPT, respectively. *Blue* or *green lines* and *symbols* represent excretion from $Muc1^{+/+}$ or $Muc1^{-/-}$ mice, respectively. TPT influenced $U_{Na}\dot{V}$ ($p < 0.01$), $U_{Phos}\dot{V}$ ($p < 0.0001$), and $U_{Ca}\dot{V}$ ($p < 0.0001$), however, the genotype-treatment interaction term was not significant by mixed effects modeling (p = NS). Error bars represent standard error. *B*, TPT induced a similar degree of hypercalcemia in Muc1$^{-/-}$ and Muc1$^{+/+}$ animals. Blood Ca^{2+} was similar in TPT-treated $Muc1^{+/+}$ and $Muc1^{-/-}$ mice (p = NS). Error bars represent SD of the mean. NSS, normal saline solution; TPT, teriparatide.
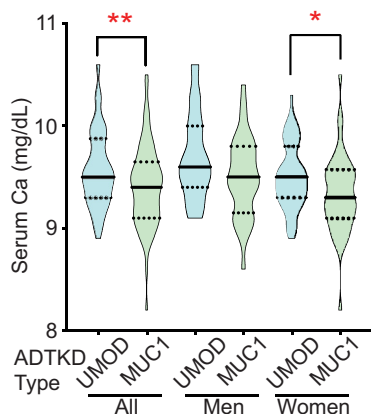
Figure 6. Plasma Ca is lower in individuals with autosomal dominant tubulointerstitial kidney disease due to *MUC1* mutation (ADTKD-MUC1) than in control individuals with autosomal dominant tubulointerstitial kidney disease due to *UMOD* mutation (ADTKD-UMOD). Violin plots representing plasma Ca extend from minimum to maximum values. *Solid lines* represent the median; *dashed lines* represent quartiles. Plasma Ca levels were lower in ADTKD-MUC1 patients than in controls (**p < 0.01 by Student's *t* test). After stratification by sex, this difference persisted in women (*p < 0.05 by Student's *t* test) but not in men (*p* = NS).

Nutrient Mixture F-12 (D6421) supplemented with 5% fetal bovine serum (Gibco/Thermo Fisher Scientific) and maintained at 37 °C in 5% CO_2. Preparation of the MDCK cell line stably transfected with human *MUC1* with 22 tandem repeats (MDCK-MUC1) was previously described (32). MDCK-MUC1 cells or nontransfected MDCK cells were plated at confluency on 12-well plastic dishes and transfected with EGFP-TRPV5 or TRPV6-Flag the following day using Lipofectamine 2000 (Invitrogen, Thermo Fisher Scientific). Plasmids encoding GFP-TRPV5 (rabbit) and TRPV6-Flag (human) were kindly provided by Chou-Long Huang (University of Iowa) and Ji-Bin Peng (University of Alabama at Birmingham), respectively. The TRPV6 cDNA was subsequently moved to pCDNA3 (Sigma-Aldrich). Endocytosis of proteins in MDCK cells was carried out as previously described (33). Briefly, cells were treated with membrane-impermeant sulfo-NHS-SS-biotin on ice and moved to a circulating water bath at 37 °C for 0, 10, or 20 min. Cells were returned to ice and surface biotin was stripped with MESNA. Cells were scraped and extracted in detergent with protease inhibitors and phosphatase inhibitors and incubated overnight at 4 °C with neutravidin-conjugated beads. Beads were washed and proteins eluted in sample buffer with β-mercaptoethanol at 60 °C for 5 min before SDS-PAGE and immunoblotting for either TRPV5, TRPV6, MUC1, or endogenous podocalyxin (see Table 2). Rabbit anti-GFP antibody (Invitrogen) was used for GFP-TRPV5 (dilution 1:4000). Rabbit anti-TRPV6 antibody was from Alomone Labs (dilution 1:1000). Armenian hamster anti-MUC1 cytoplasmic tail antibody CT2 was a gift from Sandra J. Gendler at Mayo Clinic (dilution 1:1000) (34). Mouse anti-podocalyxin antibodies 3F2/D8 (cell culture supernatant) were from Developmental Studies Hybridoma Bank (dilution 1:33). Secondary HRP-tagged antibodies were from Jackson Labs (dilution 1:10,000). Blots were developed using Bio-Rad Clarity ECL reagent (3 min) and a Bio-Rad Chemidoc. Data were quantified with Quantity One 4.6.6 software (https://www.bio-rad.com/en-us/product/quantity-one-1-d-analysis-software?ID=1de9eb3a-1eb5-4edb-82d2-68b91bf360fb).

Patch-clamp electrophysiology

HEK293-H cells were cultured with 5% CO_2 at 37 °C in Dulbecco's modified Eagle's Medium supplemented with 10% fetal calf serum, 1% penicillin/streptomycin, and 1% minimal essential medium nonessential amino acids. They were seeded on 8-mm-diameter round glass cover slips coated with poly-L-lysine and transfected using lipofectamine 2000 (Invitrogen), with 2 μg of TRPV6 and 2 μg of pIRES empty vector [GFP alone], or with 2 μg of TRPV6, 1 μg of pIRES empty vector, and 1 μg of *MUC1*. The total amount of plasmid DNA was held constant at 4 μg. The following day, cells were transferred to a chamber mounted on the stage of a Nikon inverted microscope equipped with light-emitting diodes (Thorlabs) for identification of GFP-expressing cells. Voltage clamp experiments were performed with a PC-505B patch-clamp amplifier (Warner Instruments), as described previously (35–38). Micropipettes were pulled from borosilicate glass capillary tubes (Warner Instruments) with a PP-830 puller (Narishige). Fire-polished micropipettes with a tip resistance of 1.5 to 3 MΩ were used for patch-clamp recordings. Command protocols and data acquisition were controlled by pClamp 10 (Molecular Devices). Signals were low-pass filtered at 1 kHz (4-pole Bessel filter) and digitized with a Digidata 1440A interface at 5 kHz (Molecular Devices). Whole cell recordings from HEK293-H cells were obtained at room temperature by mechanical rupture of the cell membrane in the cell-attached mode. Capacitance of the cell membrane was measured using the cell test in pClamp 10. The whole cell capacitance was then

Table 2
Antibodies used

Experiment	Antigen	Conjugation	Animal of origen	Source	Catalog no.	Dilution
Immunoblotting	GFP		Rabbit	Invitrogen	A11122	1:4000
	TRPV6		Rabbit	Alomone	ACC-036	1:1000
	MUC1 C-terminus (CT2)		Armenian hamster	Sandra J. Gendler (15)		1:2000
	podocalyxin		Mouse	DSHB	3F2/D8	1:33
Immunofluorescence microscopy	TRPV5		Rabbit	Alomone	ACC-035	1:50
	Rabbit IgG	Cy3	Goat			1:800
	Parvalbumin		Guinea Pig			1:100
	Guinea Pig IgG	Alexa-488	Goat			1:400
	TRPV6		Rabbit	Alomone Labs	Cat #: ACC-036	1:50

compensated with the amplifier. Patch pipette filling solution contained (in mM) 140 NMDG, 1 MgCl₂, 20 EGTA, and 10 Hepes, adjusted to pH 7.2 with HCl. The standard bath solution was composed of (in mM) 138 NaCl, 5 KCl, 1 MgCl₂, 2 CaCl₂, and 10 Hepes, adjusted to pH 7.4 with NaOH. Divalent cation-free (DVF) solution contained (in mM) 147 NMDG, 15 D-glucose, 10 Hepes, adjusted to pH 7.4 with HCl. After whole cell configuration was obtained in standard solution, cells were initially bathed in DVF solution for 5 min to allow proper dialysis of the cell interior. During recordings, the bath solution was replaced by a DVF solution supplemented with 2 mM CaCl₂. Solutions were delivered by continuous perfusion with a gravity-fed delivery system. Currents were monitored using ramp commands (–110 mV to +70 mV in 500 ms) applied every 5 s at a holding potential of –10 mV between ramps. All reported currents were normalized by cell capacitance and expressed as current density (pA/pF).

Animal care

Mice were housed at the University of Pittsburgh Department of Laboratory Animals. Experimental procedures were approved by the University of Pittsburgh Institutional Animal Care and Use Committee. Mice were propagated in the C57Bl/ 6J background. All experimental mice were the product of crosses between male and female *Muc1*^{+/−} mice. Genotyping was performed as previously described ([39]). All *Muc1*^{+/+} (control) mice were littermate controls. Mice were fed Prolab Isopro RMH 3000, LabDiet chow (1.09% Ca²⁺, 0.24% Mg²⁺, 0.94% K⁺, and 0.23% Na⁺) and water purified by reverse osmosis. They were maintained on a 12 h/12 h light/dark cycle.

Urine collection was performed as follows: to ensure voiding and to prevent volume depletion, animals were first injected with 7.5% (volume/body weight) sterile NSS and then placed in a metabolic cage. Urine voided in the first 30 min was discarded. Urine was then collected over the next 3.5 h. Animals were sacrificed, and bladder urine was aspirated and combined with urine collected in metabolic cages.

At time of sacrifice, mice underwent nonsurvival surgery under isoflurane anesthesia to collect blood, kidney, and duodenum specimens.

To examine urinary response to PTH receptor activation, mice were injected with the stable PTH analog, TPT. Mice were given an injection of vehicle alone (5% volume/body weight NSS, i.p.), and urine was collected in metabolic cages as six 1-h fractions. Two days later, mice were again injected with 5% body weight NSS, this time with 150 μg/kg TPT. Urine was again collected in metabolic cages as six 1-h fractions to assess urinary excretion of Na, phosphorus, and Ca.

Immunofluorescence confocal microscopy

Kidney or duodenum was placed in 4% paraformaldehyde in PBS for 16 h at 4 °C. After cryoprotecting the slices by immersion in 30% sucrose in PBS-0.02% azide, 5 μm thick cryosections were prepared as described previously ([40], [41]). Immunofluorescence labeling was subsequently performed using rabbit TRPV5 or TRPV6 antibody, followed by a

secondary goat anti-rabbit antibody coupled to Cy3 ([Table 2]). Immunolabeled tissues were mounted in *VECTASHIELD* mounting medium (Vector Laboratories) and imaged in a confocal laser scanning microscope (Leica TCS SP5, Model upright DM 6000S, Leica Microsystems Inc) using a 63× objective with identical laser settings for all samples. Immunofluorescence images were analyzed using Fiji (https://imagej. net/software/fiji/downloads), by investigators blinded to genotype ([42]). Signal intensity was measured along the length of lines drawn from the tubular or intestinal lumen, across the cell surface and into the cytoplasmic space (avoiding nuclei). Resulting line scans were normalized to maximum height and then averaged for comparison between genotypes using Igor Pro software (Wavemetrics, Inc; wavemetrics.com). Direct comparison of cytoplasmic/apical staining intensity was performed in Fiji by drawing boxes of arbitrary size within the cytoplasmic space and across the region of peak staining intensity at the cell apex.

Metabolite measurement

Whole blood electrolytes were measured using an iSTAT blood analyzer (Abbott). Plasma 1,25(OH)₂ vitamin D was measured through the Charles and Jane Pak Center for Mineral Metabolism and Clinical Research at UT Southwestern Medical Center. PTH was measured from plasma separated from whole blood by centrifugation at 4 °C in EDTA-containing tubes, flash-frozen in liquid nitrogen, and stored at −80 °C. Plasmas were thawed on ice, and PTH levels were measured in plasma diluted 1:5 using a mouse PTH ELISA (MyBioSource). Urine Na, Ca, and phosphorus were measured in samples diluted in 2% nitric acid using a PerkinElmer NeXION 300× inductively coupled mass spectrometer. Stool Ca²⁺ measurement was performed by ICP-MS following microwave assisted extraction in 6% nitric acid (Center for Applied Isotope Studies, University of GA).

Human subjects

Human data for the current study were provided by the Wake Forest Rare Inherited Kidney Disease Registry, as approved by the Wake Forest School of Medicine Institutional Review Board, in adherence with the Declaration of Helsinki ([15]). *MUC1* sequencing was performed either at the Broad Institute using mass spectrometry–based probe extension ([16]) or at the Charles University, using Illumina and SMRT methods ([17]). Plasma creatinine and total Ca levels were measured using standard clinical methods at the Wake Forest Baptist Health clinical pathology laboratory. For each individual, an average Ca and eGFR value was calculated based on the first three available measurements. Individuals were excluded if they had mean eGFR less than 60 ml/min or had nonphysiologic eGFR (greater than 200 ml/min) or Ca²⁺ (greater than 12 mg/dl or less than 8 mg/dl).

Statistics

Statistical comparisons were performed in GraphPad Prism, version 9.4.0 (graphpad.com). Outliers were identified using

the ROUT method (Q = 1%) and excluded prior to statistical analysis. Specific statistical tests used are described in figure legends.

Data availability

All methods and data are described in the article.

Abbreviations—The abbreviations used are: DVF, divalent cation-free; MDCK, Madin-Darby canine kidney; NSS, normal saline solution; PTH, parathyroid hormone; TPT, teriparatide.

References

1. Nie, M., Bal, M. S., Yang, Z., Liu, J., Rivera, C., Wenzel, A., *et al.* (2016) Mucin-1 increases renal TRPV5 activity *in vitro*, and urinary level associates with calcium nephrolithiasis in patients. *J. Am. Soc. Nephrol.* **27**, 3447–3458
2. Kim, S. K. (2018) Identification of 613 new loci associated with heel bone mineral density and a polygenic risk score for bone mineral density, osteoporosis and fracture. *PLoS One* **13**, e0200785
3. Morris, J. A., Kemp, J. P., Youlten, S. E., Laurent, L., Logan, J. G., Chai, R. C., *et al.* (2019) An atlas of genetic influences on osteoporosis in humans and mice. *Nat. Genet.* **51**, 258–266
4. Kemp, J. P., Morris, J. A., Medina-Gomez, C., Forgetta, V., Warrington, N. M., Youlten, S. E., *et al.* (2017) Identification of 153 new loci associated with heel bone mineral density and functional involvement of GPC6 in osteoporosis. *Nat. Genet.* **49**, 1468–1475
5. Estrada, K., Styrkarsdottir, U., Evangelou, E., Hsu, Y. H., Duncan, E. L., Ntzani, E. E., *et al.* (2012) Genome-wide meta-analysis identifies 56 bone mineral density loci and reveals 14 loci associated with risk of fracture. *Nat. Genet.* **44**, 491–501
6. Medina-Gomez, C., Kemp, J. P., Trajanoska, K., Luan, J., Chesi, A., Ahluwalia, T. S., *et al.* (2018) Life-course genome-wide association study meta-analysis of total body BMD and assessment of age-specific effects. *Am. J. Hum. Genet.* **102**, 88–102
7. Watanabe, K., Stringer, S., Frei, O., Umićević Mirkov, M., de Leeuw, C., Polderman, T. J. C., *et al.* (2019) A global overview of pleiotropy and genetic architecture in complex traits. *Nat. Genet.* **51**, 1339–1348
8. Patton, S., Gendler, S. J., and Spicer, A. P. (1995) The epithelial mucin, MUC1, of milk, mammary gland and other tissues. *Biochim. Biophys. Acta* **1241**, 407–423
9. Peng, J. B., Suzuki, Y., Gyimesi, G., and Hediger, M. A. (2018) TRPV5 and TRPV6 calcium-selective channels. In: Kozak, J. A., Putney, J. W., Jr., eds. *Calcium Entry Channels in Non-Excitable Cells*, CRC Press/Taylor & Francis Group, LLC, Boca Raton, FL: 241–274
10. Lee, J. W., Chou, C. L., and Knepper, M. A. (2015) Deep sequencing in microdissected renal tubules identifies nephron segment-specific transcriptomes. *J. Am. Soc. Nephrol.* **26**, 2669–2677
11. Nijenhuis, T., Hoenderop, J. G., van der Kemp, A. W., and Bindels, R. J. (2003) Localization and regulation of the epithelial Ca2+ channel TRPV6 in the kidney. *J. Am. Soc. Nephrol.* **14**, 2731–2740
12. McAuley, J. L., Linden, S. K., Png, C. W., King, R. M., Pennington, H. L., Gendler, S. J., *et al.* (2007) MUC1 cell surface mucin is a critical element of the mucosal barrier to infection. *J. Clin. Invest.* **117**, 2313–2324
13. Hoenderop, J. G., van Leeuwen, J. P., van der Eerden, B. C., Kersten, F. F., van der Kemp, A. W., Merillat, A. M., *et al.* (2003) Renal Ca2+ wasting, hyperabsorption, and reduced bone thickness in mice lacking TRPV5. *J. Clin. Invest.* **112**, 1906–1914
14. Bianco, S. D., Peng, J. B., Takanaga, H., Suzuki, Y., Crescenzi, A., Kos, C. H., *et al.* (2007) Marked disturbance of calcium homeostasis in mice with targeted disruption of the Trpv6 calcium channel gene. *J. Bone Miner. Res.* **22**, 274–285
15. Cha, S.-K., Wu, T., and Huang, C.-L. (2008) Protein kinase C inhibits caveolae-mediated endocytosis of TRPV5. *Am. J. Physiol. Renal Physiol.* **294**, F1212–F1221
16. Yates, A. J., Gutierrez, G. E., Smolens, P., Travis, P. S., Katz, M. S., Aufdemorte, T. B., *et al.* (1988) Effects of a synthetic peptide of a parathyroid hormone-related protein on calcium homeostasis, renal tubular calcium reabsorption, and bone metabolism *in vivo* and *in vitro* in rodents. *J. Clin. Invest.* **81**, 932–938
17. Bleyer, A. J., Kidd, K., Zivna, M., and Kmoch, S. (2017) Autosomal dominant tubulointerstitial kidney disease. *Adv. Chronic Kidney Dis.* **24**, 86–93
18. Brum, A. M., van der Leije, C. S., Schreuders-Koedam, M., Chaibi, S., van Leeuwen, J. P., and van der Eerden, B. C. (2018) Mucin 1 (Muc1) deficiency in female mice leads to temporal skeletal changes during aging. *JBMR Plus* **2**, 341–350
19. Christou, M. A., Ntritsos, G., Markozannes, G., Koskeridis, F., Nikas, S. N., Karasik, D., *et al.* (2020) A genome-wide scan for pleiotropy between bone mineral density and nonbone phenotypes. *Bone Res.* **8**, 26
20. Meyer, T. E., Verwoert, G. C., Hwang, S. J., Glazer, N. L., Smith, A. V., van Rooij, F. J., *et al.* (2010) Genome-wide association studies of serum magnesium, potassium, and sodium concentrations identify six loci influencing serum magnesium levels. *PLoS Genet.* **6**, e1001045
21. Liu, Y., El-Achkar, T. M., and Wu, X.-R. (2012) Tamm-Horsfall protein regulates circulating and renal cytokines by affecting glomerular filtration rate and acting as a urinary cytokine trap. *J. Biol. Chem.* **287**, 16365–16378
22. Duarte, C. G. (1968) Effects of ethacrynic acid and furosemide on urinary calcium, phosphate and magnesium. *Metabolism* **17**, 867–876
23. Rejnmark, L., Vestergaard, P., Heickendorff, L., Andreasen, F., and Mosekilde, L. (2005) Effects of long-term treatment with loop diuretics on bone mineral density, calcitropic hormones and bone turnover. *J. Intern. Med.* **257**, 176–184
24. Dumic, J., Dabelic, S., and Flögel, M. (2006) Galectin-3: an open-ended story. *Biochim. Biophys. Acta* **1760**, 616–635
25. Shan, M., Gentile, M., Yeiser, J. R., Walland, A. C., Bornstein, V. U., Chen, K., *et al.* (2013) Mucus enhances gut homeostasis and oral tolerance by delivering immunoregulatory signals. *Science* **342**, 447–453

26. Poland, P. A., Rondanino, C., Kinlough, C. L., Heimburg-Molinaro, J., Arthur, C. M., Stowell, S. R., *et al*. (2011) Identification and characterization of endogenous galectins expressed in Madin Darby canine kidney cells. *J. Biol. Chem.* **286**, 6780–6790

27. Lim, H., Yu, C. Y., and Jou, T. S. (2017) Galectin-8 regulates targeting of Gp135/podocalyxin and lumen formation at the apical surface of renal epithelial cells. *FASEB J.* **31**, 4917–4927

28. Wolf, M. T., Wu, X.-R., and Huang, C.-L. (2013) Uromodulin upregulates TRPV5 by impairing caveolin-mediated endocytosis. *Kidney Int.* **84**, 130–137

29. Lang, T., Hansson, G. C., and Samuelsson, T. (2007) Gel-forming mucins appeared early in metazoan evolution. *Proc. Natl. Acad. Sci. U. S. A.* **104**, 16209–16214

30. Duraisamy, S., Kufe, T., Ramasamy, S., and Kufe, D. (2007) Evolution of the human MUC1 oncoprotein. *Int. J. Oncol.* **31**, 671–677

31. Peng, J.-B. (2011) TRPV5 and TRPV6 in transcellular Ca 2+ transport: regulation, gene duplication, and polymorphisms in African populations. *Adv. Exp. Med. Biol.* **704**, 239–275

32. Kinlough, C. L., Poland, P. A., Gendler, S. J., Mattila, P. E., Mo, D., Weisz, O. A., *et al*. (2011) Core-glycosylated mucin-like repeats from MUC1 are an apical targeting signal. *J. Biol. Chem.* **286**, 39072–39081

33. Hanisch, F. G., Kinlough, C. L., Staubach, S., and Hughey, R. P. (2012) MUC1 membrane trafficking: protocols for assessing biosynthetic delivery, endocytosis, recycling, and release through exosomes. *Methods Mol. Biol.* **842**, 123–140

34. Croce, M. V., Isla-Larrain, M., Remes-Lenicov, F., Colussi, A. G., Lacunza, E., Kim, K. C., *et al*. (2006) MUC1 cytoplasmic tail detection using CT33 polyclonal and CT2 monoclonal antibodies in breast and colorectal tissue. *Histol. Histopathol.* **21**, 849–855

35. Montalbetti, N., and Carattino, M. D. (2021) Acid-sensing ion channels modulate bladder nociception. *Am. J. Physiol. Renal Physiol.* **321**, F587–F599

36. Montalbetti, N., Rooney, J. G., Marciszyn, A. L., and Carattino, M. D. (2018) ASIC3 fine-tunes bladder sensory signaling. *Am. J. Physiol. Renal Physiol.* **315**, F870–F879

37. Kovacs, G., Montalbetti, N., Franz, M. C., Graeter, S., Simonin, A., and Hediger, M. A. (2013) Human TRPV5 and TRPV6: key players in cadmium and zinc toxicity. *Cell Calcium* **54**, 276–286

38. Kovacs, G., Montalbetti, N., Simonin, A., Danko, T., Balazs, B., Zsembery, A., *et al*. (2012) Inhibition of the human epithelial calcium channel TRPV6 by 2-aminoethoxydiphenyl borate (2-APB). *Cell Calcium* **52**, 468–480

39. Spicer, A. P., Rowse, G. J., Lidner, T. K., and Gendler, S. J. (1995) Delayed mammary tumor progression in Muc-1 null mice. *J. Biol. Chem.* **270**, 30093–30101

40. Bouley, R., Pastor-Soler, N., Cohen, O., McLaughlin, M., Breton, S., and Brown, D. (2005) Stimulation of AQP2 membrane insertion in renal epithelial cells *in vitro* and *in vivo* by the cGMP phosphodiesterase inhibitor sildenafil citrate (viagra). *Am. J. Physiol. Renal Physiol.* **288**, F1103–F1112

41. Al-bataineh, M. M., Gong, F., Marciszyn, A. L., Myerburg, M. M., and Pastor-Soler, N. M. (2014) Regulation of proximal tubule vacuolar H(+)-ATPase by PKA and AMP-activated protein kinase. *Am. J. Physiol. Renal Physiol.* **306**, F981–F995

42. Schindelin, J., Arganda-Carreras, I., Frise, E., Kaynig, V., Longair, M., Pietzsch, T., *et al*. (2012) Fiji: an open-source platform for biological-image analysis. *Nat. Methods* **9**, 676–682